# Verification of STREAM/RAST-K for a Soluble Boron-Free Small Modular Reactor Core Using MCS

Ian Nam[a], Kyeongwon Kim[a], Hyungwoo Sohn[a], Sungju Kwon[b], Hyunsik Hong[b], Deokjung Lee[a*]
[a]*Department of Nuclear Engineering, Ulsan National Institute of Science and Technology, 50 UNIST-gil, Ulsan, 44919, Republic of Korea*
[b]*KEPCO NF, 242, Daedeok-daero 989 beon-gil, Yuseong-gu, Daejeon, 34057, Republic of Korea*
**Corresponding author: deokjung@unist.ac.kr*

***Keywords :*** soluble boron-free SMR, high-absorption burnable absorber, STREAM/RAST-K, MCS, critical rod search

## 1. Introduction

As the elimination of chemical and volume control systems in soluble-boron-free small modular reactors (SBF-SMRs) precludes the use of soluble boron, reactivity control and criticality maintenance entirely rely on burnable absorbers and mechanical control rods.

To satisfy these requirements, high-absorption burnable absorbers (HABAs) are being considered for stronger reactivity suppression. However, their large neutron absorption cross sections cause local neutron spectrum distortions, complicating the prediction of HABA depletion behavior. In addition, the frequent and continuous movement of control rods causes severe spatial variations in power and neutron spectrum throughout the core. Local spectral distortions affect whole-core leakage, power, and burnup distributions. Consequently, reliable analysis of HABA-loaded SBF-SMR cores requires accurate prediction of critical control rod bank positions and rigorous verification of the overall whole-core analysis capability against high-fidelity reference solutions.

Against this background, this study evaluates the capability and accuracy of the two-step deterministic STREAM/RAST-K (ST/RK) developed by the Computational Reactor Physics & Experiment (CORE) lab at Ulsan National Institute of Science & Technology (UNIST) [1, 2] for HABA-loaded SBF-SMR core analysis, including the prediction of critical CR bank positions. For this purpose, first-cycle whole-core depletion calculations were performed under two control rod conditions, all-rods-out (ARO) and a control-rod-inserted condition (CR case). For the CR case, the critical control rod bank positions were searched by RAST-K and evaluated using MCS [3], a continuous-energy Monte Carlo code developed by the UNIST CORE lab. To evaluate the accuracy of ST/RK, key core parameters, including the effective multiplication factor ($k_{eff}$), axial shape index (ASI), peaking factor ($F_q$), distributions of power, burnup, and coolant temperature were compared with reference solutions generated using MCS. The comparison of the whole-core depletion results for the ARO and CR cases assesses the validity and reliability of ST/RK as an analysis framework for the SBF-SMR and provides a basis for its future application to practical core design.

## 2. Modeling

### *2.1 Design Data*

The analyzed core is a representative SBF-SMR configuration developed with reference to the SMR design and fuel assembly data reported in [4]. Based on publicly reported design data, the reference model in this study employs a 69-assembly core configuration with Westinghouse-type 17×17 fuel-assembly lattices. The core has an active height of 240 cm, includes HABAs, and is surrounded by heavy metal reflectors. The same SBF-SMR model was consistently employed in both ST/RK and MCS.

### *2.2 Methodologies*

The STREAM calculations employed the pin-based pointwise energy slowing-down method, the U-238 resonance up-scattering correction with the Doppler broadening rejection correction, and a semi-predictor/corrector depletion scheme [5]. RAST-K performed three-dimensional whole-core depletion calculations for both the ARO and CR cases using a multigroup nodal diffusion solver and the group constants generated by STREAM. The quadratic depletion method was applied to HABA depletion in both ST/RK and MCS. Both codes used equilibrium xenon and the TH1D multi-physics solver with a gap conductance of 10,000 W/m²K. Table I summarizes the calculation conditions for the ST/RK and MCS.

Table I: Calculation conditions for ST/RK and MCS.

| Code | Parameter | Value |
|---|---|---|
| **ST/RK** | Burnup steps | 42 to 20 MWd/kgU |
| | MOC ray spacing | 0.01 cm |
| | MOC angles | 96 azimuthal / 6 polar |
| **MCS** | Criticality cycles | 15 inactive + 30 active |
| | Histories per cycle | 2.00E+06 |
| | Total histories | 9.00E+07 |
| | Burnup steps | 42 steps to 20 MWd/kgU |
| **STREAM & MCS** | Ring meshes | UO2: 3, HABA: 15 |
| **RAST-K & MCS** | Axial meshes | 24 |

For each MCS calculation, 15 inactive and 30 active cycles were run with $2.0 \times 10^6$ neutron histories per cycle, for a total of $9.0 \times 10^7$ histories. This resulted in an absolute standard deviation of approximately 10 pcm for $k_{\text{eff}}$. For the CR case, RAST-K searched the positions of four regulating banks, R1–R4, to achieve criticality. The resulting bank positions were subsequently used as input to MCS to independently evaluate the RAST-K-predicted critical state. These calculations are referred to as RAST-K CR-search and MCS CR-input, respectively.

## 3. Results

Relative power, coolant temperature, and burnup distributions were averaged over each assembly and axial mesh before being normalized to 1.0. ST/RK was evaluated against MCS using $k_{\text{eff}}$ differences at the RAST-K-searched critical CR bank positions, together with the maximum and root-mean-square relative errors in the spatial distributions.

### *3.1 Effective Multiplication Factor ($k_{eff}$)*

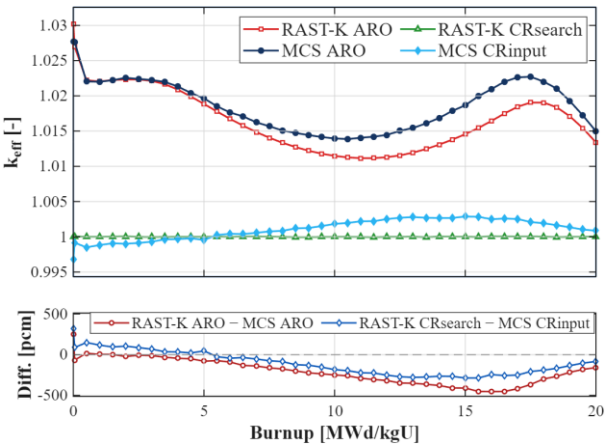



Fig. 1. $k_{\text{eff}}$ comparison (top) and difference (bottom) for the ARO and CR cases.

Fig. 1 and Table II and III summarize the $k_{\text{eff}}$ results for the ARO and CR cases. ST/RK follows the MCS depletion trend in both cases. In the ARO, the maximum $k_{\text{eff}}$ difference is 453 pcm at 16.0 MWd/kgU. For the CR case, the maximum difference between the RAST-K CR-search and MCS CR-input results is 322 pcm at BOC, with MCS standard deviations of 6–9 pcm.

Table II: Representative ARO $k_{\text{eff}}$ comparison between ST/RK and MCS.

| BU | RAST-K | MCS | Diff. | MCS SD |
|---|---|---|---|---|
| *(MWd/kgU)* | $k_{eff}$ | $k_{eff}$ | *(pcm)* | *(pcm)* |
| **0.0** | 1.03023 | 1.02772 | 251 | 15 |
| **5.0** | 1.01885 | 1.01965 | -80 | 9 |
| **10.0** | 1.01148 | 1.01396 | -248 | 6 |
| **15.0** | 1.01456 | 1.01866 | -410 | 9 |
| **20.0** | 1.01340 | 1.01498 | -158 | 9 |

Table III: Representative RAST-K CR-search positions and corresponding MCS CR-input results.

| BU | Bank position | MCS | Diff. | MCS SD |
|---|---|---|---|---|
| *(MWd/kgU)* | *R4/R3/R2/R1 (cm)* | $k_{eff}$ | *(pcm)* | *(pcm)* |
| **0.0** | 12/111/231/252 | 0.99677 | 322 | 9 |
| **5.0** | 52/172/252/252 | 0.99954 | 46 | 8 |
| **10.0** | 89/209/252/252 | 1.00183 | -184 | 9 |
| **15.0** | 71/191/252/252 | 1.00287 | -286 | 6 |
| **20.0** | 140/213/252/252 | 1.00086 | -84 | 7 |

### *3.2 Axial Shape Index (ASI)*

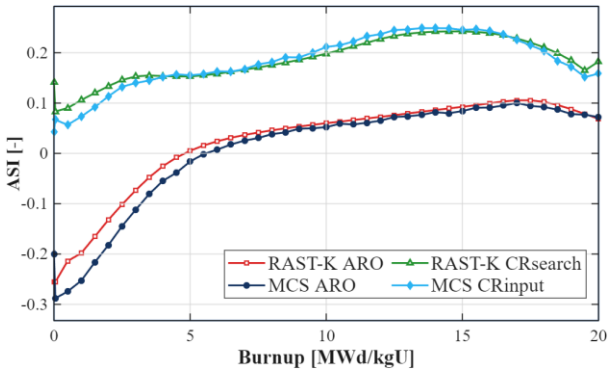



Fig. 2. ASI comparison for the ARO and CR cases.

Fig. 2 compares the ASI calculated by the two code systems. ST/RK generally agrees well with the ASI variation obtained by MCS for ARO and CR cases. For the ARO, the maximum ASI difference is 0.060 at 0.5 MWd/kgU, and differences persist up to approximately 8 MWd/kgU. For the CR case, the ASI difference reaches its maximum value of 0.099 at BOC but decreases as burnup progresses. In particular, the ASI remains positive throughout most of the burnup range in the CR case because regulating-bank insertion suppresses power in the upper half of the core and shifts the axial power balance downward. Because ASI is determined by the relative balance between the lower and upper half core powers, small differences in the predicted rod bank effect or axial power distribution can lead to relatively large ASI differences.

### *3.3 Peaking Factor ($F_q$)*

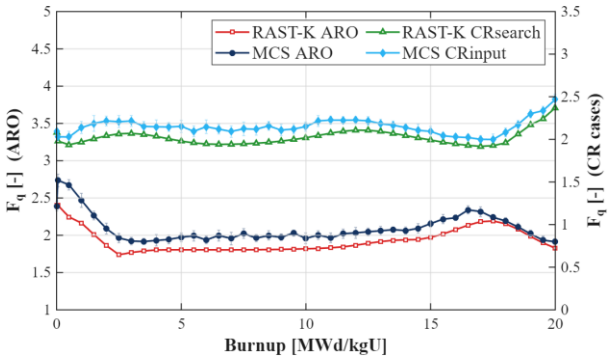



Fig. 3. $F_q$ comparison for the ARO and CR cases.

Fig. 3 compares the $F_q$. ST/RK and MCS show similar trends for both the ARO and CR cases. The maximum difference is 0.431 at 0.5 MWd/kgU for the ARO case and 0.202 at 6.0 MWd/kgU for the CR case.

### *3.4 Radial Power Distribution*

| ARO BOC 0.00 MWd/kgU | | | | |
|---|---|---|---|---|
| 1.187 | 1.149 | 1.208 | 1.152 | 0.774 |
| 1.183 | 1.149 | 1.217 | 1.159 | 0.769 |
| 0.44 | 0.38 | 0.16 | 0.12 | 0.26 |
| 0.39 | 0.04 | -0.79 | -0.60 | 0.69 |
| 1.149 | 1.151 | 1.189 | 1.074 | 0.742 |
| 1.149 | 1.154 | 1.196 | 1.078 | 0.734 |
| 0.35 | 0.26 | 0.11 | 0.11 | 0.24 |
| 0.07 | -0.27 | -0.60 | -0.42 | 1.07 |
| 1.208 | 1.189 | 1.139 | 1.005 | 0.611 |
| 1.214 | 1.195 | 1.143 | 1.003 | 0.603 |
| 0.19 | 0.13 | 0.05 | 0.12 | 0.25 |
| -0.51 | -0.44 | -0.39 | 0.19 | 1.31 |
| 1.152 | 1.074 | 1.005 | 0.715 | RAST-K |
| 1.158 | 1.076 | 1.002 | 0.711 | MCS |
| 0.11 | 0.10 | 0.12 | 0.19 | MCS Rel. SD [%] |
| -0.54 | -0.19 | 0.23 | 0.54 | Rel. Error [%] |
| 0.774 | 0.742 | 0.611 | Rel. Diff. [%] | |
| 0.769 | 0.735 | 0.604 | RMS | 0.66 |
| 0.16 | 0.14 | 0.23 | Min | -0.79 |
| 0.73 | 1.03 | 1.25 | Max | 1.31 |

| CR cases BOC 0.00 MWd/kgU | | | | |
|---|---|---|---|---|
| 0.712 | 0.688 | 0.819 | 1.288 | 1.018 |
| 0.722 | 0.688 | 0.816 | 1.302 | 1.015 |
| 0.22 | 0.11 | 0.17 | 0.12 | 0.11 |
| -1.35 | -0.02 | 0.45 | -1.03 | 0.23 |
| 0.688 | 0.505 | 1.069 | 1.264 | 0.997 |
| 0.688 | 0.519 | 1.073 | 1.277 | 0.987 |
| 0.14 | 0.08 | 0.09 | 0.10 | 0.09 |
| -0.03 | -2.65 | -0.39 | -1.00 | 0.94 |
| 0.819 | 1.069 | 1.230 | 1.288 | 0.855 |
| 0.813 | 1.072 | 1.229 | 1.286 | 0.838 |
| 0.13 | 0.06 | 0.06 | 0.05 | 0.09 |
| 0.79 | -0.30 | 0.03 | 0.11 | 2.01 |
| 1.288 | 1.264 | 1.288 | 0.981 | RAST-K |
| 1.300 | 1.276 | 1.284 | 0.969 | MCS |
| 0.09 | 0.08 | 0.08 | 0.09 | MCS Rel. SD [%] |
| -0.90 | -0.97 | 0.25 | 1.23 | Rel. Error [%] |
| 1.018 | 0.997 | 0.855 | Rel. Diff. [%] | |
| 1.018 | 0.987 | 0.838 | RMS | 1.07 |
| 0.10 | 0.06 | 0.09 | Min | -2.65 |
| -0.02 | 0.93 | 2.01 | Max | 2.01 |

| ARO MOC 10.00 MWd/kgU | | | | |
|---|---|---|---|---|
| 1.209 | 1.177 | 1.209 | 1.143 | 0.776 |
| 1.234 | 1.198 | 1.218 | 1.141 | 0.758 |
| 0.12 | 0.11 | 0.14 | 0.10 | 0.10 |
| -1.97 | -1.75 | -0.70 | 0.15 | 2.28 |
| 1.177 | 1.174 | 1.188 | 1.069 | 0.740 |
| 1.199 | 1.193 | 1.198 | 1.063 | 0.723 |
| 0.08 | 0.06 | 0.06 | 0.05 | 0.08 |
| -1.80 | -1.59 | -0.83 | 0.58 | 2.47 |
| 1.209 | 1.188 | 1.130 | 0.986 | 0.605 |
| 1.222 | 1.200 | 1.132 | 0.975 | 0.588 |
| 0.10 | 0.06 | 0.08 | 0.08 | 0.12 |
| -1.00 | -0.97 | -0.19 | 1.14 | 2.88 |
| 1.143 | 1.069 | 0.986 | 0.700 | RAST-K |
| 1.146 | 1.066 | 0.976 | 0.689 | MCS |
| 0.12 | 0.06 | 0.07 | 0.10 | MCS Rel. SD [%] |
| -0.31 | 0.27 | 0.99 | 1.53 | Rel. Error [%] |
| 0.776 | 0.740 | 0.605 | Rel. Diff. [%] | |
| 0.766 | 0.725 | 0.591 | RMS | 1.54 |
| 0.15 | 0.10 | 0.10 | Min | -1.97 |
| 1.33 | 2.08 | 2.40 | Max | 2.88 |

| CR cases MOC 10.00 MWd/kgU | | | | |
|---|---|---|---|---|
| 0.976 | 0.951 | 1.118 | 1.231 | 0.883 |
| 0.979 | 0.951 | 1.124 | 1.238 | 0.875 |
| 0.16 | 0.11 | 0.12 | 0.11 | 0.09 |
| -0.33 | -0.03 | -0.50 | -0.55 | 0.97 |
| 0.951 | 0.796 | 1.142 | 1.160 | 0.845 |
| 0.951 | 0.796 | 1.148 | 1.157 | 0.834 |
| 0.13 | 0.09 | 0.09 | 0.07 | 0.08 |
| -0.03 | 0.01 | -0.51 | 0.20 | 1.38 |
| 1.118 | 1.142 | 1.180 | 1.102 | 0.694 |
| 1.129 | 1.146 | 1.184 | 1.098 | 0.685 |
| 0.13 | 0.07 | 0.08 | 0.11 | 0.11 |
| -0.94 | -0.33 | -0.34 | 0.37 | 1.33 |
| 1.231 | 1.160 | 1.102 | 0.796 | RAST-K |
| 1.241 | 1.164 | 1.101 | 0.795 | MCS |
| 0.12 | 0.09 | 0.09 | 0.10 | MCS Rel. SD [%] |
| -0.85 | -0.38 | 0.08 | 0.10 | Rel. Error [%] |
| 0.883 | 0.845 | 0.694 | Rel. Diff. [%] | |
| 0.880 | 0.838 | 0.686 | RMS | 0.68 |
| 0.13 | 0.07 | 0.09 | Min | -0.94 |
| 0.34 | 0.90 | 1.18 | Max | 1.38 |

| ARO EOC 20.00 MWd/kgU | | | | |
|---|---|---|---|---|
| 1.271 | 1.252 | 1.201 | 1.094 | 0.774 |
| 1.250 | 1.234 | 1.186 | 1.094 | 0.789 |
| 0.14 | 0.09 | 0.10 | 0.15 | 0.13 |
| 1.66 | 1.50 | 1.29 | 0.05 | -1.90 |
| 1.252 | 1.235 | 1.181 | 1.049 | 0.739 |
| 1.236 | 1.221 | 1.172 | 1.051 | 0.748 |
| 0.09 | 0.09 | 0.07 | 0.06 | 0.11 |
| 1.31 | 1.15 | 0.80 | -0.17 | -1.26 |
| 1.201 | 1.181 | 1.115 | 0.966 | 0.592 |
| 1.192 | 1.174 | 1.114 | 0.972 | 0.603 |
| 0.10 | 0.06 | 0.07 | 0.06 | 0.10 |
| 0.78 | 0.62 | 0.05 | -0.65 | -1.82 |
| 1.094 | 1.049 | 0.966 | 0.682 | RAST-K |
| 1.094 | 1.056 | 0.975 | 0.699 | MCS |
| 0.08 | 0.07 | 0.08 | 0.11 | MCS Rel. SD [%] |
| 0.02 | -0.64 | -0.95 | -2.44 | Rel. Error [%] |
| 0.774 | 0.739 | 0.592 | Rel. Diff. [%] | |
| 0.788 | 0.750 | 0.603 | RMS | 1.28 |
| 0.10 | 0.08 | 0.10 | Min | -2.44 |
| -1.77 | -1.44 | -1.79 | Max | 1.66 |

| CR cases EOC 20.00 MWd/kgU | | | | |
|---|---|---|---|---|
| 1.233 | 1.190 | 1.175 | 1.108 | 0.811 |
| 1.245 | 1.192 | 1.164 | 1.103 | 0.819 |
| 0.12 | 0.11 | 0.09 | 0.10 | 0.12 |
| -0.96 | -0.17 | 0.95 | 0.48 | -1.04 |
| 1.190 | 1.093 | 1.172 | 1.074 | 0.778 |
| 1.191 | 1.059 | 1.166 | 1.073 | 0.788 |
| 0.12 | 0.07 | 0.08 | 0.06 | 0.10 |
| -0.05 | 3.24 | 0.51 | 0.10 | -1.35 |
| 1.175 | 1.172 | 1.125 | 0.985 | 0.627 |
| 1.161 | 1.163 | 1.122 | 0.990 | 0.640 |
| 0.11 | 0.08 | 0.07 | 0.09 | 0.10 |
| 1.22 | 0.71 | 0.26 | -0.55 | -2.05 |
| 1.108 | 1.074 | 0.985 | 0.711 | RAST-K |
| 1.099 | 1.069 | 0.989 | 0.728 | MCS |
| 0.09 | 0.09 | 0.08 | 0.10 | MCS Rel. SD [%] |
| 0.82 | 0.53 | -0.45 | -2.37 | Rel. Error [%] |
| 0.811 | 0.778 | 0.627 | Rel. Diff. [%] | |
| 0.815 | 0.785 | 0.640 | RMS | 1.24 |
| 0.17 | 0.10 | 0.07 | Min | -2.37 |
| -0.47 | -0.93 | -1.96 | Max | 3.24 |

Fig. 4. ARO (left) and CR cases (right) radial power distribution comparison.

Fig. 4 compares the normalized assembly-wise radial power distributions at BOC, MOC, and EOC for both ARO and CR cases. For the ARO, the maximum relative differences and RMS errors are 1.31% and 0.66% at BOC, 2.88% and 1.54% at MOC, and 1.66% and 1.28% at EOC, respectively.

For the CR case, the corresponding values are 2.01% and 1.07% at BOC, 1.38% and 0.68% at MOC, and 3.24% and 1.24% at EOC. The largest discrepancies occur at MOC for the ARO and at EOC for the CR case, and the RMS errors remain at or below 1.54% across all cases.

### *3.5 Radial Burnup Distribution*

| ARO MOC 10.00 MWd/kgU | | | | |
|---|---|---|---|---|
| 12.454 | 12.091 | 12.500 | 11.683 | 7.865 |
| 12.697 | 12.301 | 12.663 | 11.716 | 7.731 |
| -1.91 | -1.71 | -1.29 | -0.28 | 1.73 |
| 12.091 | 12.074 | 12.300 | 11.006 | 7.537 |
| 12.308 | 12.265 | 12.436 | 11.003 | 7.381 |
| -1.76 | -1.56 | -1.10 | 0.03 | 2.12 |
| 12.500 | 12.300 | 11.700 | 10.142 | 6.187 |
| 12.666 | 12.441 | 11.758 | 10.060 | 6.032 |
| -1.31 | -1.14 | -0.50 | 0.81 | 2.58 |
| 11.683 | 11.006 | 10.142 | 7.199 | |
| 11.716 | 11.005 | 10.059 | 7.087 | |
| -0.28 | 0.02 | 0.82 | 1.58 | Rel. Diff. [%] |
| 7.865 | 7.537 | 6.187 | RMS | 1.51 |
| 7.738 | 7.378 | 6.030 | Min | -1.91 |
| 1.64 | 2.16 | 2.60 | Max | 2.60 |

| CR cases MOC 10.00 MWd/kgU | | | | |
|---|---|---|---|---|
| 8.671 | 8.462 | 10.195 | 12.436 | 9.212 |
| 8.753 | 8.489 | 10.278 | 12.490 | 9.123 |
| -0.94 | -0.31 | -0.81 | -0.43 | 0.98 |
| 8.462 | 6.559 | 11.247 | 12.047 | 8.927 |
| 8.490 | 6.634 | 11.317 | 12.081 | 8.805 |
| -0.33 | -1.13 | -0.62 | -0.28 | 1.38 |
| 10.195 | 11.247 | 12.230 | 11.673 | 7.473 |
| 10.274 | 11.311 | 12.303 | 11.650 | 7.351 |
| -0.77 | -0.57 | -0.59 | 0.20 | 1.66 |
| 12.436 | 12.047 | 11.673 | 8.600 | |
| 12.501 | 12.085 | 11.659 | 8.547 | |
| -0.52 | -0.31 | 0.12 | 0.62 | Rel. Diff. [%] |
| 9.212 | 8.927 | 7.473 | RMS | 0.85 |
| 9.136 | 8.819 | 7.365 | Min | -1.13 |
| 0.83 | 1.23 | 1.47 | Max | 1.66 |

| ARO EOC 20.00 MWd/kgU | | | | |
|---|---|---|---|---|
| 25.259 | 24.628 | 25.001 | 23.422 | 15.834 |
| 25.688 | 25.001 | 25.251 | 23.436 | 15.610 |
| -1.67 | -1.49 | -0.99 | -0.06 | 1.44 |
| 24.628 | 24.499 | 24.527 | 21.891 | 15.095 |
| 25.007 | 24.829 | 24.728 | 21.842 | 14.823 |
| -1.52 | -1.33 | -0.81 | 0.22 | 1.84 |
| 25.001 | 24.527 | 23.240 | 20.219 | 12.275 |
| 25.261 | 24.739 | 23.309 | 20.079 | 12.029 |
| -1.03 | -0.86 | -0.30 | 0.70 | 2.05 |
| 23.422 | 21.891 | 20.219 | 14.259 | |
| 23.448 | 21.859 | 20.085 | 14.124 | |
| -0.11 | 0.14 | 0.67 | 0.96 | Rel. Diff. [%] |
| 15.834 | 15.095 | 12.275 | RMS | 1.22 |
| 15.634 | 14.828 | 12.039 | Min | -1.67 |
| 1.28 | 1.80 | 1.96 | Max | 2.05 |

| CR cases EOC 20.00 MWd/kgU | | | | |
|---|---|---|---|---|
| 18.363 | 18.010 | 21.394 | 24.806 | 18.282 |
| 18.533 | 18.062 | 21.510 | 24.832 | 18.163 |
| -0.91 | -0.29 | -0.54 | -0.10 | 0.66 |
| 18.010 | 14.503 | 22.708 | 23.782 | 17.596 |
| 18.068 | 14.515 | 22.789 | 23.780 | 17.429 |
| -0.32 | -0.08 | -0.35 | 0.01 | 0.96 |
| 21.394 | 22.708 | 24.134 | 22.842 | 14.508 |
| 21.508 | 22.778 | 24.216 | 22.794 | 14.370 |
| -0.53 | -0.31 | -0.34 | 0.21 | 0.96 |
| 24.806 | 23.782 | 22.842 | 16.647 | |
| 24.852 | 23.793 | 22.819 | 16.660 | |
| -0.18 | -0.04 | 0.10 | -0.08 | Rel. Diff. [%] |
| 18.282 | 17.596 | 14.508 | RMS | 0.51 |
| 18.195 | 17.453 | 14.397 | Min | -0.91 |
| 0.48 | 0.82 | 0.78 | Max | 0.96 |

Fig. 5. ARO (left) and CR cases (right) radial burnup distribution comparison at MOC and EOC.

Fig. 5 compares the radial burnup distributions at MOC and EOC. For ARO, the maximum relative difference and RMS error are 2.60% and 1.51% at MOC, and 2.05% and 1.22% at EOC, respectively. For CR case, the corresponding values are 1.66% and 0.85% at MOC, and 0.96% and 0.51% at EOC, respectively. The RMS errors decrease from MOC to EOC in both cases, indicating improved agreement as depletion progresses. A comparison of the EOC patterns shows that the CR case yields lower burnup in the central fuel assemblies and higher burnup in the outer assemblies adjacent to the reflector relative to the ARO. This trend reflects the cumulative effect of the changes in radial power distribution induced by regulating-bank insertion.

### *3.6 Axial Coolant Temperature Distribution*

Fig. 6 – Fig. 8 compare the axial coolant temperature distributions at BOC, MOC, and EOC for ARO and CR cases. The ST/RK results match well with MCS over the entire core height in both cases. For the ARO, the maximum axial absolute temperature differences are 1.18, 0.71, and 0.78 K at BOC, MOC, and EOC, respectively. For the CR case, the corresponding peak differences are 1.07, 1.92, and 0.62 K. The same constant inlet coolant temperature was applied in both the ST/RK and MCS calculations throughout the depletion cycle, and the resulting outlet temperature differences ranged from 0.685 to 0.775 K for ARO and from 0.373 to 0.621 K for CR case. Overall, ST/RK consistently captures the axial coolant temperature profiles throughout the depletion cycle.

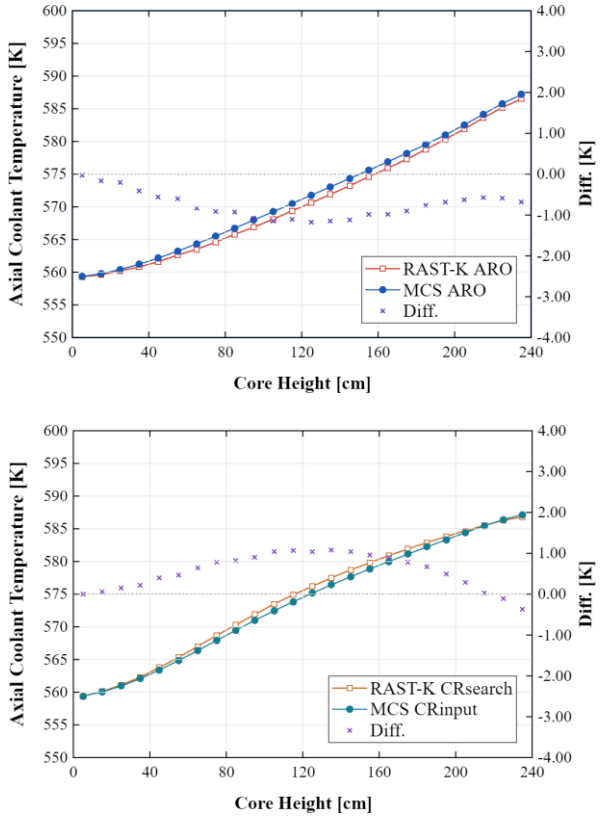



Fig. 6. ARO (top) and CR cases (bottom) axial coolant temperature distribution comparisons at BOC.

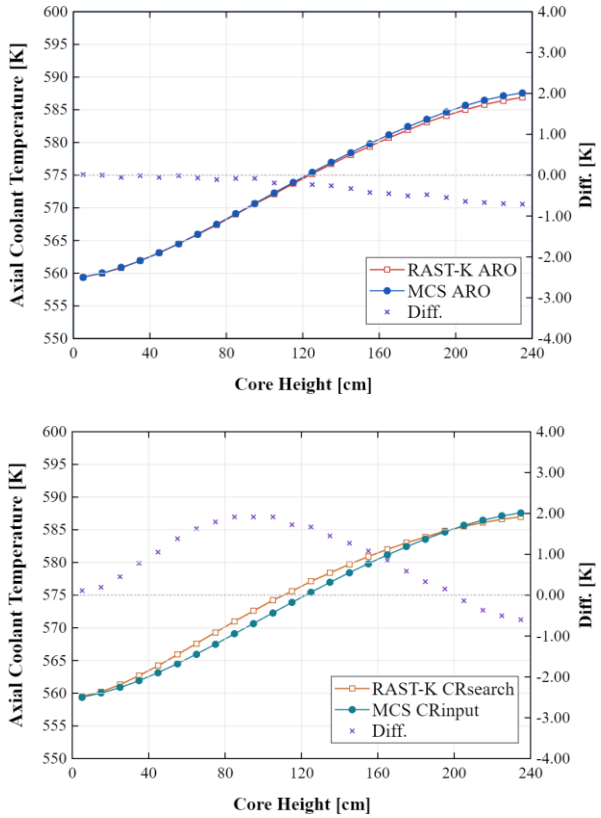



Fig. 7. ARO (top) and CR cases (bottom) axial coolant temperature distribution comparisons at MOC.

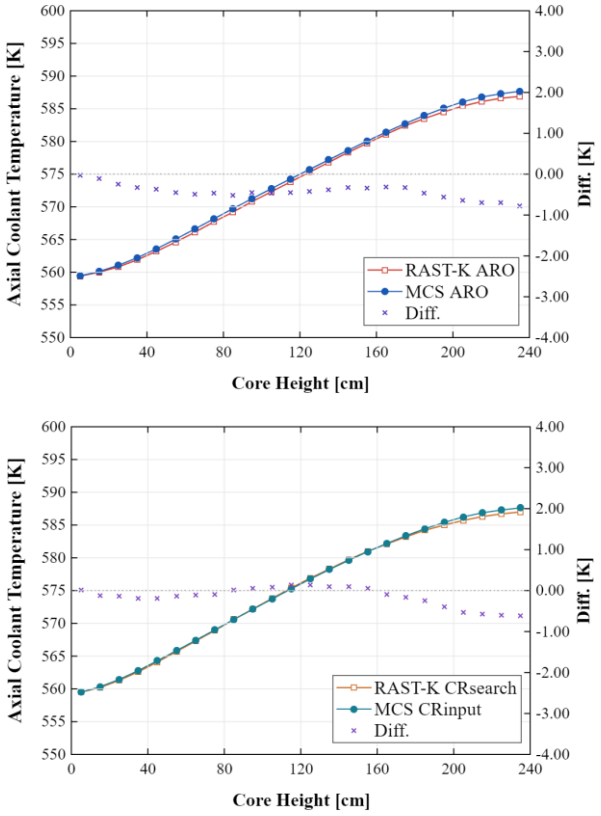



Fig. 8. ARO (top) and CR cases (bottom) axial coolant temperature distribution comparison at EOC.

The radial coolant temperature distributions also show agreement between ST/RK and MCS. For the ARO, the assembly-wise absolute temperature differences range from 0.59 to 1.09 K at BOC, from 0.50 to 0.97 K at MOC, and from 0.05 to 0.20 K at EOC.

For the CR case, corresponding ranges are 0.56–1.92 K at BOC, 0.18–0.72 K at MOC, and 0.06–0.21 K at EOC. The radial differences generally decrease with burnup for both operating conditions, and ST/RK captures the assembly-wise coolant temperature fields throughout the cycle.

## 4. Conclusion

ST/RK whole-core depletion results for the ARO and CR cases were compared with the corresponding MCS results for a representative first-cycle SBF-SMR problem. In the ARO, the maximum $k_{eff}$ difference is 453 pcm at 16.0 MWd/kgU, and the maximum ASI and $F_q$ differences are 0.060 and 0.431, respectively, both at 0.5 MWd/kgU. For ARO distributions, the maximum radial-power and radial-burnup differences are 2.88% and 2.60%, respectively, while the maximum radial and axial coolant temperature differences are 1.09 and 1.18 K, respectively. For the CR case, the maximum $k_{eff}$ difference between the RAST-K CR-search and MCS CR-input results is 322 pcm at 0.0 MWd/kgU, while the maximum ASI and $F_q$ differences are 0.099 and 0.202, respectively. The maximum radial-power and radial-burnup differences are 3.24% and 1.66% respectively,

while the maximum radial and axial coolant temperature differences are both 1.92 K.

Although the ST/RK code system was originally developed for large-scale reactors and has demonstrated high accuracy, within a $k_{eff}$ discrepancy of 200 pcm across conventional commercial PWRs and benchmarks, such as APR1400, VERA, and BEAVRS [1], its simulations for the SBF-SMR core exhibit slightly larger discrepancies. These remaining quantitative differences appear to be primarily attributed to three physical characteristics of the SBF-SMR core. These include the extensive use of HABAs that induce severe local spectrum distortion, the compact core size that significantly increases neutron leakage, and the presence of heavy metal reflectors.

Therefore, future work will focus on systematically analyzing and identifying the underlying physical causes of these increased discrepancies in the SBF-SMR core.

## Acknowledgements

This work was supported by the Innovative Small Modular Reactor Development Agency grant funded by the Korea Government (RS-2023-00265742).

## REFERENCES

[1] J. Choe, S. Choi, P. Zhang, J. Park, W. Kim, H. C. Shin, H. S. Lee, J.-E. Jung, and D. Lee, "Verification and validation of STREAM/RAST-K for PWR analysis," Nuclear Engineering and Technology, vol. 51, no. 2, pp. 356–368, 2019.

[2] K. Kim, D. Yun, W. Kim, S. J. Kwon, S. Fathurrahman, and D. Lee, "Explicit and simplified modeling of in-core instrument for emitter region reaction rate calculation using STREAM/RAST-K," Nuclear Engineering and Technology, vol. 58, 104243, 2026.

[3] H. Lee, W. Kim, P. Zhang, M. Lemaire, A. Khassenov, J. Yu, Y. Jo, J. Park, and D. Lee, "MCS–A Monte Carlo particle transport code for large-scale power reactor analysis," Annals of Nuclear Energy, vol. 139, 107276, 2020.

[4] J. Kim, B. H. Cho, and S. G. Hong, "Applicability evaluation of enriched gadolinium as a burnable absorber in assembly level for boron-free i-SMR core," Transactions of the Korean Nuclear Society Spring Meeting, Jeju, Korea, May 19–20, 2022.

[5] H. Sohn, W. Kim, and D. Lee, "Preliminary Analysis on Accuracy of Strong Burnable Absorber Depletion," Transactions of the Korean Nuclear Society Autumn Meeting, Changwon, Korea, October 24–25, 2024.